Accepted Manuscript

A Novel Microfluidic Resistive Pulse Sensor with Multiple Voltage Input Channels and a Side Sensing Gate for Particle and Cell Detection

Tong Zhou, Yongxin Song, Yapeng Yuan, Dongqing Li

PII: S0003-2670(18)31407-7

DOI: https://doi.org/10.1016/j.aca.2018.11.049

Reference: ACA 236426

To appear in: *Analytica Chimica Acta*

Received Date: 4 October 2018

Accepted Date: 26 November 2018

Please cite this article as: T. Zhou, Y. Song, Y. Yuan, D. Li, A Novel Microfluidic Resistive Pulse Sensor with Multiple Voltage Input Channels and a Side Sensing Gate for Particle and Cell Detection, *Analytica Chimica Acta*, https://doi.org/10.1016/j.aca.2018.11.049.

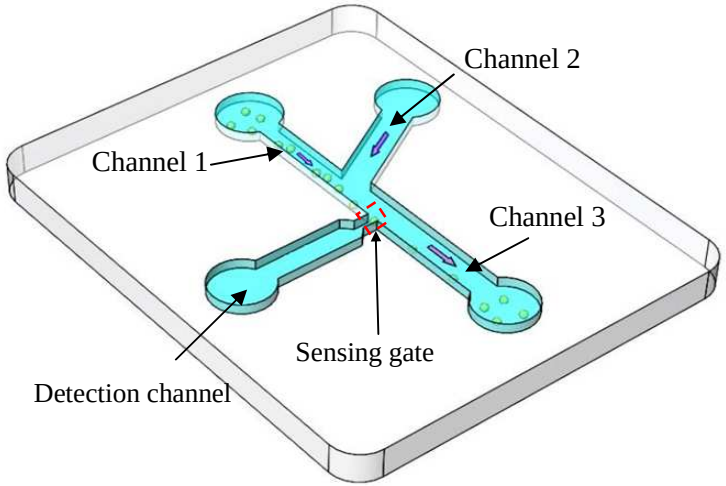

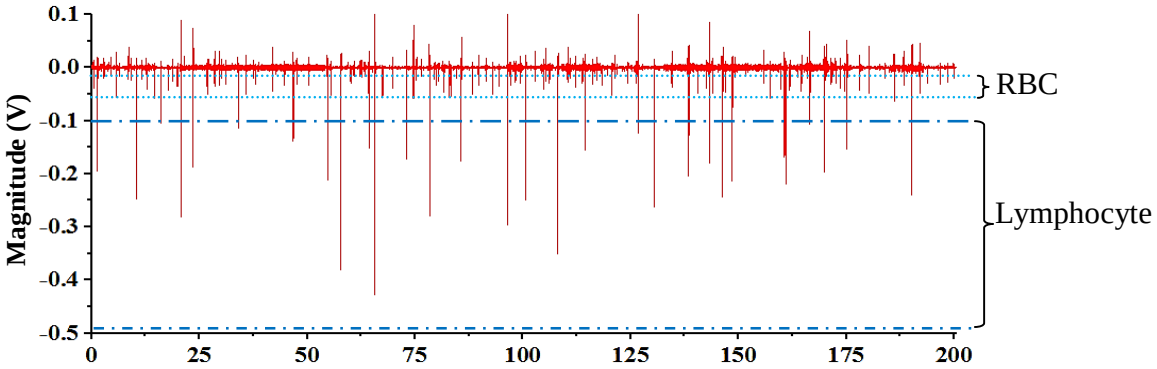

A Novel Microfluidic Resistive Pulse Sensor with Multiple Voltage Input Channels and a Side Sensing Gate for Particle and Cell Detection

Tong Zhou[1,+], Yongxin Song[1,+], Yapeng Yuan[1] and Dongqing Li[*2]

1 Department of Marine Engineering, Dalian Maritime University, Dalian, 116026, China

2 Department of Mechanical and Mechatronics Engineering, University of Waterloo, Waterloo, ON, N2L 3G1, Canada

*Corresponding author: E-mail: dongqing@uwaterloo.ca

[+] Tong Zhou and Yongxin Song contributed equally to this work.

Abstract

Traditionally, a resistive pulse sensor (also known as Coulter counter) works by letting a particle pass through a small orifice in an electrolyte solution. The detection sensitivity mainly relies on the volume ratio of the particle to the orifice. This paper presents a novel resistive pulse sensor which has a sensing orifice located on the side wall of a microchannel. In this way, the sensor can detect and count particles (or cells) without requiring particles (or cells) passing through the sensing gate. An equation was derived to relate the magnitudes of the detected signals and the electrical resistances. Results show that the magnitudes of the detected signals can be increased by applying voltages from more than one voltage input channels simultaneously. Under the same conditions, the magnitudes of the detected signals become larger when the diameters of particles are larger. Higher detection sensitivity can be obtained simply by increasing either the magnitudes of the applied voltages or the number of the voltage input channels, or reducing the opening of the side sensing gate to a size that is even smaller than the diameter of the particle. Due to the high detection sensitivity, detection of 1 μm particles by a relatively large sensing gate of 5×10×10 μm (width × length × height) was successfully demonstrated with a signal to noise ratio (S/N) of approximately 3. This sensor was also applied to detect and count human red blood cells and lymphocyte cells. Results show that this method can clearly distinguish the cells with different sizes based on the pre-determined-thresholds. Because this sensor does not require cells to pass through the sensing gate, the channel clogging problem can be avoided. More importantly, the detection sensitivity can be tuned by applying different voltages without fabricating a smaller sensing gate.

Keywords: Resistive pulse sensing; Multiple voltage input channels; Side sensing gate; Cell detection

Introduction

Coulter counter, also known as the resistive pulse sensor, is one very popular method for particle or cell detection, counting and sizing. Invented by Coulter [1], this method works by using a very small insulating orifice filled with an electrolyte solution and by applying a DC electric field across the orifice. When a particle passes through the orifice, a temporary change of electrical resistance is caused due to the difference in the resistivity of the particle (or cell) and the resistivity of the electrolyte solution. With a proper measurement system, the resistance change can be measured as either a current pulse or a voltage pulse. The numbers and the magnitudes of the pulses represent the numbers and the sizes of the particles (or cells) passing through the orifice [2]. Due to its high accuracy and simplicity, the Coulter principle has been widely used in flow cytometry [3] for cell analysis. While the flow cytometer is a powerful instrument, it is bulky and expensive, and requires a relatively large sample volume.

Recently, microfluidic and nanofluidic resistive pulse sensors have attracted the interests of researchers [4-19] due to their advantages such as simple construction, low cost and portability [20-27]. For a microfluidic or nanofluidic resistive pulse sensor, several different designs and detection approaches have been developed for improving the sensitivity or the throughput. One very popular approach is to place electrodes across the sensing channel [15, 28-35]. In these sensors, the size of the "orifice" used for particle sensing depends on both the size of the sensing channel and the distance between the two electrodes. In order to fabricate a very small orifice, advanced micro-fabrication facilities are needed. Furthermore, complicated operations and expensive equipment are generally involved in fabricating the electrodes. To avoid fabricating the micro-electrodes, Ag/AgCl electrodes were used for applying voltages to the fluidic circuit [36-38]. The Ag/AgCl electrodes are widely used in the field of electrochemistry. A key benefit of using Ag/AgCl electrodes is that it can reduce the electrode polarization problem which is adverse to the sensitivity of the resistive pulse sensor [31, 39-40].

Since the resistance change produced by a particle passing through the "orifice" is very small, some advanced signal processing instruments, such as lock-in amplifier [28,41], or impedance

analyzer [38,42] are generally needed with the aim to increase the detection sensitivity. Instead of directly monitoring the ionic current change caused by a particle, Li et.al [43-45] employed a commercial metal-oxide-semiconductor field-effect transistor (MOSFET) to monitor the drain current modulation corresponding to the change of the gate voltage due to a particle passing through the "orifice". Because the MOSFET has a high sensitivity, a volume ratio (particle to the orifice) of 0.006% was detected.

In order to increase the detection sensitivity without using sophisticated and expensive instruments, a differential resistive pulse sensing method was developed [7,10,19,46-49]. The novelty of this sensor is to reduce the noises by designing two identical detection channels and inputting the signals to a differential amplifier. In this way, most of the noises can be cancelled and thus the signal to noise ratio (S/N) was greatly improved. The experimental results showed that this method is very effective in cancelling the noises and improving S/N [48,50].

There are also some other resistive pulse sensors (RPS) with novel designs that enables high detection sensitivity. One of them is the so-called flow-focusing type which uses focusing solutions with a much bigger electric resistivity to narrow the "orifice" [13,35-36,51-52]. The novel idea of this method is to generate a virtual wall using the higher-electric-resistance focusing solution. Due to the high resistivity of the focusing solution, most of the electric field lines will be concentrated in the narrowed sample solution which is electrically more conductive. This is equivalent to having a narrower sensing orifice. Therefore, the less conductive the focusing solution is, the more sensitive the sensor is. For example, a clear difference in the signal magnitudes of 1 μm and 2 μm polystyrene particles was detected due to the increased sensitivity and discrimination by using an oil-surfactant mixture as the focusing solution [35]. For the above studies, it should be noted, the focusing solution can decrease only the width of the sensing region. For the length of the sensing region, it is still determined by the distance between the electrodes placed across the "orifice", which relies on using microfabrication equipment. Recently, Liu et al. [16] developed another new flow-focusing method that can be used to improve the sensitivity of a differential RPS sensor. For this method developed by Liu, the focusing solution is electrokinetically transported in the focusing channel. In this way, the electric field within the

sensing gate is concentrated and thus the detection sensitivity is significantly improved. As a result, detection of 1μm polystyrene particles with a relatively large physical sensing gate of 30×40×10 μm (width × length × height) was successfully demonstrated.

In summary, for the existing microfluidic or nanofluidic RPS sensors, they all require the to-be-detected-particles to pass through the sensing orifice. As a result, the orifice may be clogged by the particles or the impurities in the liquid. This problem becomes serious when a small orifice is used to detect nanoparticles or DNA molecular. Moreover, for the performance of a microfluidic RPS, most of the studies are focused on the effects of the size of the sensing orifice on the detection sensitivity. Less attention is given to the influence of the channel size and configuration on the sensitivity.

Generally, a traditional RPS has only one straight channel with a small orifice. Theoretically, the output signal (voltage) will be increased with the increase in the applied voltage. The noise level, however, will also be increased at the same time. This will decrease the S/N (sensitivity). Furthermore, for the traditional RPS, the electric field within the whole channel will be evenly increased when increasing the applied voltage. This will also decrease the voltage output. The best case is to focus most of the electric field within the small orifice, which can be achieved by designing several parallel input channel and only one small orifice (in this study). Currently, there are no reports on the effects of channel resistances and number of voltage input channels on voltage output.

This paper presents a novel resistive pulse sensor which employs multiple voltage input channels and a sensing gate located on one side of the microchannel wall. This RPS sensor can detect and count particles (or cells) without requiring particles (or cells) to pass through the sensing gate. An equation was derived to correlate the detected signal and the electrical resistances of different channel branches. The influence of several parameters on the performance of this sensor were analyzed and experimentally verified. Detecting and distinguishing red blood cells and lymphocyte cells was also performed to demonstrate the size discrimination ability of this novel sensor.

2. Working Principle and performance evaluation

2.1 Detection system and working principle

The novel microfluidic RPS sensor (Figure 1(a)), consists of a microfluidic chip, an electrical resistor, a DC power supply, a differential amplifier (AD620) and a LabView® based data acquisition device (NI USB6259, NI, USA). The microfluidic chip, shown in Figure 1(b), has three voltage- input channels (named as channel 1, channel 2 and channel 3, respectively), one detecting channel and the corresponding wells. At the joint of the detection channel and the three voltage-input channels, there is a small sensing gate. In addition, to conduct the applied electrical voltage, channel 1 is also used for loading particles or cells, and channel 2 is used for transporting sheath flow to let the particles move as close to the sensing gate as possible.

In each of the wells, there is a Pt electrode used for connecting the DC power supply. Specifically, the Pt electrode in the well of the detecting channel is linked to the negative end of the DC power supply. The other three wells are linked to the positive end of the DC power supply. The electrodes of channel 1 and 3 are for applying additional electric fields which are used to increase the sensitivity of this sensor. That is why the channels 1, 2 and 3 are referred as the voltage-input channels. Moreover, an electrical resistor is mounted between the positive end of the DC power supply and the Pt electrodes of channels 1, 2 and 3. The voltage signal across the electrical resistor (R) is outputted to the amplifier and the data acquisition module.

For the system shown in Figure 1, the wells of the channels 1, 2 and 3 should be filled with PBS buffer firstly. After adding sample solution into the well of channel 1 and applying a voltage through the Pt electrode, the particles will be transported to pass by the sensing gate. During this process, the electric resistance of the system will be dramatically changed at the moment when the particle is near the entrance of the sensing gate. Accordingly, the voltage across the resistor is changed and will be detected by the system. In this way, particle detection is achieved.

The resistance change caused by a particle near the entrance of the sensing gate can be understood by the corresponding electric circuit as is shown schematically in Figure 2. Theoretically, the electrical resistance of a channel (R_c) full of an electrolyte solution is given by:

$$R_c = \rho \frac{4L}{\pi D^2} \tag{1}$$

Where ρ is the sample solution's resistivity, D and L are the diameter and length of the channel respectively. When there are no particles passing by the sensing gate, as is shown in Figure 2 (a), the total electric resistance of the system (R_T) can be calculated as:

$$R_T = R_{\mathrm{m}} + R_s + R_d \tag{2-a}$$

$$\frac{1}{R_m} = \frac{1}{R_{\mathrm{m},1}} + \frac{1}{R_{m,2}} + \frac{1}{R_{m,3}} \tag{2-b}$$

where R_s and R_d are the resistances of the sensing gate and the detection channel; $R_{m,1}$, $R_{m,2}$ and $R_{m,3}$ are the resistances of the channel 1, channel 2 and channel 3, respectively; R_m is the total resistance of these three channels which are in parallel connection.

When a voltage difference V is applied across the channels, the voltage drop across the electric resistor with a resistance of R_r can be expressed as:

$$V_r = \frac{R_r}{R_m + R_s + R_d + R_r} V \tag{3}$$

When an insulating particle passes by the entrance of the sensing gate, it will have two positions relative to the sensing gate. One extreme case is that the particle adheres to the entrance of the sensing gate at one moment. If we consider such a particle and the sensing gate as a whole, the length and the diameter of the "new" sensing gate are increased and decreased, respectively. Normally this will increase the electric resistance of the sensing gate due to the dominant role of the diameter in determining the resistance. Another case is that the particle is near the sensing gate (with a gap between the particle and the sensing gate). For this case, it can be considered as adding another resistor in serial with R_s. In conclusion, the passing of a particle will increase the electric resistance of the system, as is shown in Figure 2 (b). This is similar to the classic Coulter counter, where the increased resistance is due to the displacement of the same volume of the electrolyte solution from the sensing gate by the passing-through particle.

Assuming the increased resistance by the passing of a particle is ΔR, the new voltage drop across the resistor (V_r') can be calculated as:

$$V_r' = \frac{R_r}{R_m + R_s + R_d + R_r + \Delta R} V \tag{4}$$

Based on Eq. (3) and Eq. (4), therefore, the voltage change across the resistor (ΔV_r) after a particle passes by the sensing gate is:

$$\Delta V_r = -\frac{\Delta R \cdot R_r}{(R_m + R_s + R_d + R_r)(R_m + R_s + R_d + R_r + \Delta R)} V \tag{5}$$

For the measurement system shown in Figure 1 (a), the voltage drop over the resistor is inputted to the differential amplifier with a gain of A. The final output signal should be the sum of the voltage change generated by a particle passing by the sensing gate and the system noise, and can be written theoretically as:

$$\Delta V_{output} = \eta + A\frac{\Delta R \cdot R_r}{(R_m + R_s + R_d + R_r)(R_m + R_s + R_d + R_r + \Delta R)} V \tag{6}$$

where η is the system noise.

As can be seen from Eq. (6), each particle will output a voltage signal when passing by the sensing gate. Such a change can be measured as a signal pulse with the measurement system shown in Figure 1(a). In this way, particle detection and counting can be achieved.

2.2 Performance Evaluation and Comparison

1) Performance evaluation

To evaluate the working performance of this novel sensor, the effects of several parameters, such as the channel resistances, the applied voltages, the resistance of the electric resistor, on the magnitudes of the output signals are evaluated in this section. To do such an evaluation, the following simplifications for Eq.(6) are assumed: (1) The system noise η is always the same under different channel sizes and thus is ignored in the following analysis; (2) The gain of the amplifier *A* is set as 1.

Let us define four new parameters *a*, *b*, *c* and *d* as the following:

Relative resistance of the voltage input channels $a = \frac{R_m}{R_s}$ (7-a)

Relative resistance of the detection channel $b = \frac{R_d}{R_s}$ (7-b)

Relative resistance of the electric resistor $c = \frac{R_r}{R_s}$ (7-c)

Relative resistance caused by the passing particle $d = \frac{\Delta R}{R_s}$ (7-c)

Eq.(6) can be rewritten as:

$$\Delta V_r = -\frac{d\,c}{(a+b+c+1)\,(a+b+c+d+1)}V \quad (8)$$

Figure 3 displays the dependence of the magnitudes of the output signals on the different parameters of *a, b, c* and *d*. (Table 1 shows the parameter values used in the simulation). These figures clearly demonstrate the different effects exerted by the different resistances on the magnitudes of the signals. As can be seen from Figure 3(a), with the increase of the applied voltage, the signal magnitude also increases under the same resistance ratio *a*. This is because the voltage shared by the resistor is proportional to the total applied voltage. A larger applied voltage causes a larger voltage drop across the resistor, as well as the voltage change when a particle goes through the sensing gate. However, the noises from the applied power supply, which is input into the system and cannot be quantified and reflected in Figure 3 (a), will also increase with the increased voltage applied across the channels. As a result, the S/N will be determined by the competition between the magnitude of the applied voltage and the noises.

One much more important discovery shown in Figure 3 (a) is that the output of the signal magnitude decreases with the increasing relative resistance of the voltage input channels *a* under the same applied voltage. Since *a* can be decreased by decreasing the total resistance of the voltage input channels (R_m), it means that the signal magnitude (also the S/N) can be increased by decreasing the total resistance of the voltage input channels (R_m). According to the Eq. (1) and Eq. (2-b), the total resistance of the voltage input channels is determined both by the sizes and the numbers of the voltage input channels. When the channel sizes are kept the same, adding more parallel voltage input channels will results in a smaller R_m and thus a larger magnitude of the output signal. Such a result is due to the fact that the resistance of the sensing gate (R_s) should be

dominant among all of the channel resistances. Otherwise, the resistance change generated by a particle will not be large enough to generate a detectable signal. Decreasing the electrical resistances of the voltage input channels can be considered as an alternative way of improving the electrical resistance of the sensing gate.

As regards to the electrical resistance of the detection channel, as is shown in Figure 3(b), it has the same effect on the signal output as the resistance of the voltage input channels. Because the resistances of the voltage input channels and the detection channel are connected in series, they should have the same effect on the voltage distribution of the system.

It should be noted that there is a maximum for the signal magnitude when the relative resistance of the resistor, *c*, is about 80 (Figure 3 (c)). This is due to the coupled effect between the resistance change (ΔR) caused by the passing particle and the resistance of the resistor (R_r): the change of R_r will change the value of ΔR which will also change the voltage drop shared by R_r. Therefore, the relationship between R_r and the signal output should be described by a quadratic equation. This relationship is particularly helpful for selecting an appropriate resistor in order to obtain maximum signal output. Figure 3 (d) shows the effect of the resistance change produced by a particle on the magnitude of the signal output. It's clear that the magnitude of the signal increases linearly with the increase of the relative resistance *d* caused by a passing particle. The reason is that the larger the ΔR , the less the voltage drop across the resistor will be when a particle passes by the sensing gate. Since the voltage drop shared by the resistor is the same when there are no particles passing by the sensing gate, as a result, the changed voltage across the resistor is larger when a particle is passing over the sensing gate.

2) Comparison with the traditional Coulter counter

For the traditional Coulter counter, it relies on the electric resistance change (ΔR) which is closely related with the volume ratio of the particle and the orifice [2]. In general, a larger ΔR requires a larger volume ratio of the particle to the orifice. At any events, however, the diameter of the particle should be smaller than that of the orifice in order to let the particle pass through the orifice.

Different from the traditional Coulter counter, the novel RPS sensor developed in this paper works by letting the moving particle cut the electric lines at the entrance of the sensing gate, and does not require the particle to go through the sensing gate. Currently, there are no equations that can calculate the resistance change produced by a particle moving over the sensing gate. Theoretically, such a resistance change should also be influenced by the size ratio of the particle to the sensing gate, which reflects the interference of the particle with the electric field. However, the size ratio is no longer limited by the size of the sensing gate because the particle does not need to be smaller than the width of the sensing gate. For this sensor, one extreme case is that the sensing gate is so small that it is temporarily blocked by a large particle at the entrance and the path (the detection channel) to the negative electrode is cut off, and thus the system becomes electrically open. As a result, no electrical current goes through the system and the voltage across the resistor is zero (V_r'=0, in Eq. (4)). A signal of maximal magnitude would be detected in such a case. Therefore, the magnitudes of the detected signals can be continually increased until the sensing gate is totally blocked by the particle. That is to say, the S/N of this sensor can be tuned by adjusting the volume of the sensing gate without considering the dimension of the particle.

3. Experiments

3.1 Chip Design and Fabrication

For the microfluidic chip shown in Figure 1 (b), the width and length of its sensing orifice is 5 μm and 10 μm respectively. The detection channel is 200 μm wide and 2 mm long. For channel 1, the width is 10 μm and the length is 2 mm, respectively. The width and length of the channel 2 are 200 μm and 5 mm. For the channel 3, its width and length are 200 μm and 5 mm. For the height of the chip, it is either 10μm (for smaller particle detection) or 21μm (for larger particle and blood cell detection). Different sizes of sensing gates were used for detecting different particles and cells and specified in the corresponding figure legends.

The configuration of the microfluidic chip was designed and transformed to a chromium plate as a mask firstly. Using the soft lithography method[53], the masters with a height of 10 μm and 21 μm for PDMS chip prototyping were fabricated on a silicon substrate (4” N/PHOS, Montco Silicon Technology Inc., Spring City, PA) using the negative photo-resist of SU-8 3010 (MicroChem Co.,

Newton, MA) and SU-8 3025 (MicroChem Co., Newton, MA) respectively. To fabricate the PDMS chip, liquid PDMS (Sylgard 184, Dow Corning, USA) and curing agent (a mass ratio of 10:1) were mixed together and then degassed in a vacuum oven (Isotemp model 280A, Fisher Scientific, Pittsburgh, PA, USA) for at least half an hour. Afterwards, the PDMS mixture was poured onto the master and heated at 80^{o}C in another oven (Isotemp model 280A, Fisher Scientific, Pittsburgh, PA, USA) for 2~3 hours. The firm PDMS layer was then peeled off from the master and the wells were punched on the PDMS layer. The final step is to make the PDMS layer and a glass slide (25.66 × 75.47 × 1.07 mm, CITOGLAS, China) bonded firmly by using a plasma cleaner (HARRICK PLASMA, Ithaca, NY, USA).

3.2 Sample preparation

To test the detection sensitivity of this novel RPS sensor, polystyrene particles (Fluka, Shanghai, China) of different sizes, 1μm, 2μm, 3μm, 4μm, 5μm and 7 μm in diameter, were used. For each of the particle sample, it was prepared by adding 2.5 μL pure sample solution (with a concentration of 2%) into 1×PBS buffer (pH =7.5) to decrease the concentration to be about 0.033‰.

To demonstrate the ability of this sensor on biological sample detection and size discrimination, a diluted red blood cell sample and peripheral blood lymphocyte sample prepared from a venous blood sample were measured. To obtain a pure red blood cell sample, 1 mL of venous blood sample, obtained from an anonymous healthy human donor, was added into a 1.5mL centrifugal tube and then was centrifuged under 3000rps (664xg) for 5 minutes. Afterwards, 200μL RBCs were collected from the bottom of the centrifugal tube and diluted 200 times with PBS buffer (pH =7.5). The peripheral blood lymphocyte cells were separated from a venous blood sample (1 mL) by using the Lymphocyte Separation Medium (Solarbio, Beijing, China) and diluted with 1mL PBS buffer (pH =7.5). Base on the concentration of red blood cell (7-11×10^{8}/mL) and lymphocyte (1-3×10^{6}/mL) in an healthy adult person and the above dilution procedures, the concentrations of red blood and lymphocyte samples are estimated to be in the range of 3.5-5.5×10^{6}/mL and 1-3×10^{6}/mL respectively.

3.3 Experimental procedure

To begin an experiment, the wells of the channel 1, channel 2 and the detection channel were added with 20 μL PBS buffer (pH =7.5). Then 10 μL PBS buffer (pH =7.5) solution was injected into the well of channel 3. Afterwards, 2.5 μL of sample solution was loaded into the well of channel 1.

The next step should be to add some additional buffer solution to the well of channel 2. By doing so, different liquid levels will be established between the wells of channel 1, channel 2 and detection channel and the well of channel 3. Thus, a pressure-driven flow will be generated towards the wells of the detection channel and channel 3 and the particles and cells will be hydraulically focused against the side sensing gate. In this study, the best added volume of buffer solution to the well of channel 2 was determined based on lots of experiments and were found to be 7 μL and 4.5μL for polystyrene particle sample and blood cell sample respectively. In this way, the distance between the particles (cells) and the side sensing gate was controlled to be as close as possible (See movie 1).

Finally, Pt electrodes were inserted into the wells and DC voltages were applied across the channels. The gain of the amplifier (A) was adjusted to 100. To make sure whether the signals were generated by the particles or cells, all of the particles or cells passing by the sensing gate were observed under an optical microscope (Nikon Eclipse Ti, Nikon, Japan) during the experiments. All experiments were conducted at room temperature (20±1 ℃). For each measurement, at least five signals were measured and then averaged to obtain the final signal magnitude under each experimental condition. Since the main purpose is to demonstrate the performance of the new sensor, the experiments ran only for several minutes to get enough signals to analyze their magnitudes. In practice, the duration of the detection depends on the volume of the sample that needs to be analyzed.

4. Results and Discussions

4.1 Detecting particles of different sizes

To verify that particles can be detected without going through the sensing gate, firstly the 5 μm and 7 μm particles were measured by a sensing gate of 5 ×10×10μm (Width × Length × Height). The sizes of the channels are specified in Section 4.1. Figure 4 shows the typical trajectories of 5 μm around the sensing gate during the measurements and the detected signals generated by the 5

μm and 7 μm polystyrene particles by applying an electric field of 20V/cm from the three voltage-input channels using the measurement system shown in Figure 1 (a). It's clear from Figure 4(a) that all of the 5 μm particles were focused to pass by the side sensing gate by the pressure-driven flow from Channel 2. As regards to the detected signals, shown in Figure 4 (b), each downward signal with a magnitude larger than 0.25V was produced by the 5μm polystyrene particle. The upward peaks were produced by the customer-developed Labview smoothing program which is used to avoid signal drifting. The downward signals whose magnitudes are very low are caused by the system noises.

From Figure 4 (b) we can find that the magnitudes of the detected signals, with a range of 0.25V to 0.36V, are not uniform. Such variations of signal magnitude are not due to the size differences of the particles, because the deviation from the average particle size is less than 0.1μm. It is due to the different positions of the particles passing by the sensing gate. It is not difficult to understand that a particle moving closer to the sensing gate will disturb more electric field lines (and hence the electric current) passing from the sensing gate to the detection channel, and thus generate a larger signal than that of a particle passing not-so-closely by the sensing gate. The distance of the particles near the sensing gate is determined by the electroosmotic flows and the pressure-driven sheath flow in the channels and the dielectrophoretic force around the sensing gate. Due to the slightly varying flow rates from channel 2 (due to the change of the liquid level in channel 2), there will be some differences for the focused position of the particles at the side sensing gate, which causes the variations in signal magnitudes. In practice, syringe pumps can be applied which can provide much stable focusing effect and thus much uniform signals. However, as demonstrated in Figure 4 (b), the noise level is only about 0.008V with the signal magnitudes ranging from 0.25V to 0.36V. Therefore, the S/N is between 31 and 45. Such a high S/N ratio clearly demonstrates the powerfulness and effectiveness of this novel RPS sensor for particle detection and counting.

Figure 4 (c) shows the signals generated by the 7μm particles. It's clear that the 7μm particles generated downward signals with a magnitude larger than 0.58V (the noise level is about 0.009V). Since the averaged signal magnitude (based on the repeated results) is 0.92V, therefore, the S/N

ratio is about 102. This higher S/N, compared with that of the 5μm particles, is due to the much larger electric resistance change caused by the 7 μm particle than that of the 5μm particle. It should be noted that, for this chip, the sensing gate size is 5 ×10 × 10μm (Width × Length × Height). Therefore, the 7 μm particles cannot pass through the sensing gate. The results of this study demonstrate the obvious advantage of this sensor over the traditional Coulter counter: particle detection is no longer limited by using a sensing gate whose width should be larger than the diameter of the particle.

The signals shown in Figure 4 are generated by relatively large particles. To evaluate the sensitivity of this novel sensor, the same detection system used for 5μm and 7μm particles detection (the same microfluidic chip and the same applied electric field) was employed to detect 1μm particles. The measured signals are shown in Figure 5 (a). It's interesting to find that there are upward peaks which are generated by the particles. For the downward peaks, their magnitudes rang from 0.017V to 0.028V with an averaged S/N of about 2.88. For these signals, they are generally characterized with a double-peak shape, as is typically shown in Figure 5 (b)-(d). For the double-peak signals, the downward and upward peaks represent the resistance-increasing and resistance-decreasing processes respectively. Such a double-peak signal represents a complex interaction of the particle with the electric field and was reported previously [54-57]. Generally, this phenomenon was prominent in sub-micron and nanoscale and can be attributed to the ionic concentration polarization effect [54]. For the signals shown in Figure 5, the most possible reason might be the 'end effects' of the sensing gate [56-57]. Due to the unstable trajectory of the particle under both the electroosmotic flow and the pressure-driven sheath flow, the interaction is also unstable which makes the orders of the upward peak and downward peak seem to be random.

4.2 Determining detection thresholds and discriminating particles in a mixed sample solution

Reliably determining the threshold value, i.e., the magnitude range of the detected signals is important for accurate particle detection and counting. For this sensor, the electric field around the sensing gate is non-uniform and the distance of the particles from the entrance of the sensing gate is likely different for different particles. As a result, the magnitudes of the measured signals for particles of the same size may not be the same. In this paper, the thresholds of the signal

magnitudes are determined by measuring a relatively larger number of particles.

To obtain the thresholds, the signals generated by a pure 3 μm polystyrene particle solution and a pure 5μm polystyrene particle solution were measured separately. Figure 6 shows the signal frequencies under different magnitudes. It's clear that the 3 μm and 5μm particles will generate signals with clearly different magnitudes. For example, the signal magnitudes for the 3 μm particles are between 0.05V ~ 0.12V and 80% is between 0.07 ~ 0.09V. For the 5 μm particles, the magnitude is larger than 0.2V and 80% is between 0.22 ~ 0.31V. Based on the above results, the thresholds for the 3μm particles and 5μm particles can be reasonably set as 0.05V ~ 0.12V and 0.2V ~ 0.4V, respectively. Figure 7 shows the typical detected signals for a mixed particle solution which is composed of 3 μm and 5 μm polystyrene particles. The dashed lines are the thresholds determined in Figure 6. Based on the thresholds, therefore, the signals which fall into the two pairs of dashed lines should be the 3 μm particles and 5 μm particles, respectively. Figure 8 presents the signal distributions for the particles (show in Figure 7) based on the pre-determined thresholds. It's clear that the two kinds of particles can be clearly distinguished based on the thresholds obtained by measuring the single sized particles. Therefore, this novel method can be used reliably to discriminate particles of different diameters in the sample solution.

4.3 Dependence of the signal magnitudes on the number of the voltage input channels

As is clearly demonstrated in Figure 3 (a), decreasing the resistances of the voltage input channels can increase the magnitudes of the detected signals. Since the voltage-input channels are connected in parallel, the total channel resistance can be changed by selectively applying DC voltages across the three voltage-input channels. Figure 9 shows the typical signals when the 5 μm particles pass by a sensing gate of 5×10×10 μm (width × length × height) with a voltage of 25.5V applied from different voltage input channels. It's clear that there is no detected signal when only channel 1 was applied a voltage (Figure 9 (a)). When applying the same voltage from both channel 1 and channel 2 simultaneously, as is shown in Figure 9 (b), there are downward signals with magnitudes ranging from 0.09~0.13V. When all of the three channels are applied with a voltage of

25.5V, the magnitudes of the detected signals were increased to about 0.33V, as is clearly shown in Figure 9 (c). The above experimental results agree well with the theoretical results shown in Figure 3 (a).

4.4 Dependence of the signal magnitudes on the electric fields

As is predicted by Eq. (6), the applied voltages across the channels (also the electric field intensity for a given chip) can influence the magnitudes of the detected signals. In this section, experimental results will be demonstrated. To verify this point, we measured the signals generated by 5μm particles moving over a sensing gate of 5 ×10 × 21 μm (width × length × height).

Table 2 summarizes the experimental results and the dependence of the signal magnitudes on the electric fields is plotted in Figure 10. It's easy to see that the averaged magnitudes of the signal increase almost linearly with the applied electric fields. The correlation coefficient (R^2) is 0.822. For example, the magnitude increases from 0.056V to 0.15V as the electric field is boosted from 6.7V/cm to 32.4V/cm. This agrees well with the theoretical prediction by the Eq. (6). It should be noted that the error bar is relatively larger under larger applied electric field. This is due to the larger dielectrophoretic (DEP) force exerted on the particles under the larger electric field. Under the DEP force, the particles will be pushed away from the entrance of the sensing gate and thus cause larger distance from the sensing gate under larger electric field. This is also one reason that the correlation coefficient (R^2) is not large.

4.5 Dependence of the signal magnitudes on particle size

Generally, the size of the particle to be detected by the resistive pulse sensor can greatly influence the magnitude of the detected signal. For this novel sensor, the dependence of the magnitudes of signals on particle sizes cannot be theoretically predicted and should be experimentally measured. Table 3 summarizes the experimental results and the dependence of the signal magnitudes on the sizes of the particles is plotted in Figure 11. As expected, the averaged magnitudes of the signals increase with the increase in the diameters of the particles. With this experimentally obtained curve, we can evaluate the magnitudes of the signals for particles of different sizes.

4.6 Detection and discrimination of red blood cells and lymphocytes

Since Coulter counter has been widely used in blood cells detection and counting, the novel sensor developed in this paper was also applied for blood cells detection. Figure 12 shows the typical signals generated by a pure red blood cell sample and a pure lymphocyte sample. About 135 red blood cells and 105 lymphocyte cells were detected as shown in this figure. It should be noted that the two much larger signals, indicated with red circles in Figure 12 (a), are most likely generated by impurities or more than one cells passing by the sensing gate at the same time.

Figure 13 shows the signal magnitude distributions of the detected signals (shown in Figure 12). From Figure 13, it's clear that the signal magnitudes of the red blood cells are between -0.01V and -0.063V. For the lymphocyte cells, the magnitudes are larger, ranging from -0.1V to -0.51V. Such a clear difference in magnitude is due to the different volume of the two kinds of cells. Therefore, we can set the thresholds for the red blood cells and lymphocyte cells as [-0.01V, -0.063V] and [-0.1V, -0.51V], respectively. Figure 14 shows the typical detected signals for the mixed blood cell sample which is composed of red blood cells and lymphocyte cells. The dashed lines are the thresholds as determined in Figure 13. Accordingly, the signals which fall into the two pairs of dashed lines should be red blood cells and lymphocyte cells, respectively. Figure 15 presents the signal distributions for the mixed blood sample based on the pre-determined thresholds from Figure 13. It's clear that the two kinds of blood cells can also be clearly distinguished based on the thresholds obtained by measuring the pure samples.

It should be noted that the word 'size discrimination' in this paper does not mean that it can give the accurate sizes of the particles or the cells. The word should be understood as that it can distinguish particles or cells of different sizes. This is true for the widely used commercial flow cytometers which cannot measure the accurate sizes of particles or cells neither.

5. Conclusions

This paper presents a novel resistive pulse sensor with multiple voltage input channels and a side sensing gate. This sensor can detect and count particles and cells without requiring them passing

through the sensing gate. An equation which relates the detected signals and the electrical resistances was derived. Based on the equation and the experimental results, it was found that the magnitudes of the detected signals increase with the increased numbers of the parallel voltage input channels and increases with the increase in the diameters of particles. The detection sensitivity can also be increased by using a sensing gate whose width is smaller than the diameter of the particle. For this sensor, the particles or cells need not to go through the sensing orifice, thus the channel clogging problem can be avoided. More importantly, detection sensitivity can be tuned by applying different voltages without changing the size of the sensing gate.

Acknowledgement

The authors wish to acknowledge financial support of National Natural Science Foundation program of China (51679023) and Liaoning BaiQianWan Talents Program to Yongxin Song; the Natural Sciences and Engineering Research Council of Canada through a research grant to D. Li, the support from Fundamental Research Funds for the Central Universities (3132016325) and from the University 111 project of China under Grant No. B08046 is greatly appreciated.

References

1 W.H. Coulter, Means for Counting Particles Suspended in a Fluid, US Pat. 2656508, 1953.

2 R.W. Deblois, C.P. Bean, Counting and sizing of submicron particles by the resistive pulse technique, Rev. Sci. Instrum. 41 (1970) 909–916.

3 A. Moldavan, Photo-Electric Technique for the Counting of Microscopical Cells, Science. 80 (1934) 188–189.

4 Y. Han, H. Wu, G. Cheng, J. Zhe, A two-stage microresistive pulse immunosensor for pathogen detection, Lab Chip. 16 (2016) 773–779.

5 M.E. Piyasena, S.W. Graves, The intersection of flow cytometry with microfluidics and microfabrication, Lab Chip. 14 (2014) 1044–1059.

6 T. Chung, H. Kim, Recent advances in miniaturized microfluidic flow cytometry for clinical use, Electrophoresis. 28 (2007) 4511–4520.

7 Y. Song, J. Yang, X. Pan, D. Li, High‐throughput and sensitive particle counting by a novel

microfluidic differential resistive pulse sensor with multidetecting channels and a common reference channel, Electrophoresis. 36 (2015) 495–501.

8 Z. Wang, S.Y. Chin, Cu.D. Chin, J. Sarik, M. Harper, J. Justman, S.K. Sia, Microfluidic CD4+ T-cell counting device using chemiluminescence-based detection, Anal. Chem. 82 (2010) 36–40.

9 D. Branton, D.W. Deamer, A. Marziali, H. Bayley, S.A. Benner, T. Butler, M.D. Ventra, S. Garaj, A. Hibbs, X.H. Huang, S.B. Jovanovich, P.S. Krstic, S. Lindsay, X.S.S. Ling, C.H. Mastrangelo, A. Meller, J.S. Oliver, Y.V. Pershin, J.W. Ramsey, R. Riehn, G.V. Soni, C.V. Tabard, M. Wanunu, M. Wiggin, J.A. Schloss, The potential and challenges of nanopore sequencing, Nat. Biotechnol. 26 (2008) 1146–1153.

10 Y. Song, H. Zhang, C. Chon, S. Chen, X. Pan, D. Li, Counting bacteria on a microfluidic chip, Anal. Chim. Acta. 681 (2010) 82–86.

11 L.T. Sexton, H. Mukaibo, P. Katira, H. Hess, S.A. Sherrill, L.P. Horne, C.R. Martin, An Adsorption-Based Model for Pulse Duration in Resistive-Pulse Protein Sensing, J.Am.Chem.Soc. 132 (2010) 6755–6763.

12 K. Kececi, L.T. Sexton, F. Buyukserin, C.R. Martin, Resistive-pulse detection of short dsDNAs using a chemically functionalized conical nanopore sensor, Nanomedicine. 3 (2008) 787–796.

13 T.R. Rodriguez, F.O. Castillo, M. Garrido, M. Arundell, A. Valencia, G. Gomila, High-speed particle detection in a micro-Coulter counter with two-dimensional adjustable aperture, Biosens. Bioelectron. 24 (2008) 290–296.

14 H. Jiang, X. Weng, D. Li, Dual-wavelength fluorescent detection of particles on a novel microfluidic chip, Lab Chip. 13 (2013) 843–850.

15 U.Hassan and R.Bashir, Coincidence detection of heterogeneous cell populations from whole blood with coplanar electrodes in a microfluidic impedance cytometer, Lab Chip. 14 (2014) 4370–4381.

16 Z. Liu, J. Li, J. Yang, Y. Song, X. Pan, D. Li, Improving particle detection sensitivity of a microfluidic resistive pulse sensor by a novel electrokinetic flow focusing method, Microfluid. Nanofluid. 21, 4 (2017).

17 J. Guo, X. Huang, C. Li, Y. Ai, Y. Kang, Dual characterization of biological cells by optofluidic microscope and resistive pulse sensor, Electrophoresis. 36 (2015) 420–423.

18 Y. Han, H. Wu, F. Liu, G. Cheng, J. Zhe, A multiplexed immunoaggregation biomarker assay

using a two-stage micro resistive pulse sensor, Biomicrofluidics. 10, 024109 (2016).

19 R. Peng, D. Li, Detection and sizing of nanoparticles and DNA on PDMS nanofluidic chips based on differential resistive pulse sensing, Nanoscale. 9 (2017) 5064–5974.

20 A. Manz, D.J. Harrison, E.M.J. Verpoorte, J.C. Fettinger, A. Paulus, H. Lüdi, Planar chips technology for miniaturization and integration of separation techniques into monitoring systems: Capillary electrophoresis on a chip, J.Chromatography A. 593 (1992) 253–258.

21 G.M. Whitesides, A.D. Stroock, Flexible methods for microfluidics, Physics Today. 54 (2001) 42–48.

22 S. Quake, The chips are down—microfluidic large-scale integration, Trends Anal. Chem. 21 (2002) XII–XIII.

23 D.J. Beebe, G.A. Mensing, G.M. Walker, Physics and Applications of Microfluidics in Biology, Annu. Rev. Biomd. Eng. 4 (2002) 261-286.

24 H.A. Stone, A.D. Stroock, A. Ajdari, Engineering flows in small devices, Annu. Rev. Fluid. Mech. 36 (2004) 381–411.

25 T. Squires, Microfluidics: Fluid physics at the nanoliter scale, Rev. Mod. Phys. 77 (2005) 977–1026.

26 G.M. Whitesides, The origins and future of microfluidics, Nature. 442 (2006) 368–373.

27 T. Sun, H. Morgan, Single-cell microfluidic impedance cytometry: a review, Microfluid. Nanofluid. 8 (2010) 423–443.

28 R.R. Trujillo, M.A. Ajine, A. Orzan, M.D. Mar, F. Larsen, C.H. Clausen, W.E. Svendsen, Label-free protein detection using a microfluidic Coulter-counter device, Sens. Actuators, B, 190 (2014) 922–927.

29 A.L. Mcpherson, G.M. Walker, A microfluidic passive pumping Coulter counter, Microfluid. Nanofluid. 9, (2010) 897–904.

30 A.V. Jagtiani, J. Zhe, J. Hu, J. Carletta, Detection and counting of micro-scale particles and pollen using a multi-aperture Coulter counter, Meas. Sci. Technol. 17 (2006) 1706–1714.

31 S. Zheng, L. Tai, Micro coulter counters with platinum black electroplated electrodes for human blood cell sensing, Biomed. Microdevices. 10 (2008) 221–231.

32 Y. Wu, X. Han, J.D. Benson, M. Almasri, Erratum: Micromachined Coulter counter for dynamic impedance study of time sensitive cells, Biomed. Microdevices. 15 (2013) 739–750.

33 J. Riordon, M. Mirzaei, M. Godin, Microfluidic cell volume sensor with tunable sensitivity, Lab Chip. 12 (2012). 3016–3019.

34 J. Riordon, M. Nash, M. Mirzaei, M. Godin, Using active microfluidic flow focusing to sort particles and cells based on high-resolution volume measurements, Microelectron. Eng. 2014, 118(5), 35–40.

35 C. Bernabini, D. Holmes, H. Morgan, Micro-impedance cytometry for detection and analysis of micron-sized particles and bacteria, Lab Chip. 11 (2011) 407–412.

36 H. Choi, C.S. Jeon, I. Hwang, J. Ko, S. Lee, J. Choo, J.H. Boo, H.C. Kim and T.D. Chung, A flow cytometry-based submicron-sized bacterial detection system using a movable virtual wall, Lab Chip. 14 (2014) 2327–2333.

37 E. Weatherall, G.R. Willmott, Applications of tunable resistive pulse sensing, Analyst. 140 (2015) 3318–3334.

38 S. Wang, Q. Wei, T. Zhu, J. Huang, M. Yu, Y. Sha, C. Xiong, J. Fang, CD4+ T Cell Counting by Impedance Measurement on a Chip with Fluidic Electrodes, Int. J. Nonlin. Sci. Num. 13 (2012) 313–317.

39 A.V. Jagtiani, J. Carletta, J. Zhe, An impedimetric approach for accurate particle sizing using a microfluidic Coulter counter, J. Micromech. Microeng. 21, 045036 (2011).

40 A.L. Richards, M.D. Dickey, A.S. Kennedy, Design and demonstration of a novel micro-Coulter counter utilizing liquid metal electrodes, J. Micromech. Microeng. 22, 115012 (2012).

41 M. Evander, A.J. Ricco, J. Morser, G.T. Kovacs, L.L. Leung, L. Giovangrandi, Microfluidic impedance cytometer for platelet analysis, Lab Chip. 13 (2013) 722–729.

42 H. Song, Y. Wang, J.M. Rosano, B. Prabhakarpandian, C. Garson, K. Pant, E. Lai, A microfluidic impedance flow cytometer for identification of differentiation state of stem cells, Lab Chip. 13.12 (2013), 2300–2310.

43 M. Sridhar, D. Xu, Y. Kang, A.B. Hmelo, L.C. Feldman, D. Li, D. Li, Experimental characterization of a metal-oxide-semiconductor field-effect transistor-based Coulter counter, J. Appl. Phys. 103, 104701 (2008).

44 D. Xu, Y. Kang, M. Sridhar, A.B. Hmelo, L.C. Feldman, D. Li, D. Li, Wide-spectrum, ultrasensitive fluidic sensors with amplification from both fluidic circuits and metal oxide

semiconductor field effect transistors, Appl. Phys. Lett. 91, 013901 (2007).

45 J. Sun, C.C. Sowers, E.M. Boczko, Li. D, Measurement of the volume growth rate of single budding yeast with the MOSFET-based microfluidic Coulter counter, Lab Chip.10 (2010) 2986–2993.

46 X. Wu, Y. Kang, Y. Wang, D. Xu, D. Li, D. Li, Microfluidic differential resistive pulse sensors, Electrophoresis. 29 (2008) 2754–2759.

47 X. Wu, C. Chon, Y. Wang, Y. Kang, D. Li, Simultaneous particle counting and detecting on a chip, Lab Chip. 8 (2008) 1943–-1949.

48 Y. Song, H. Zhang, C. Chon, X. Pan, D. Li, Nanoparticle detection by microfluidic Resistive Pulse Sensor with a submicron sensing gate and dual detecting channels-two stage differential amplifier, Sens. Actuators, B. 155 (2011) 930–936.

49 D. Shi, J. Guo, L. Chen, C. Xia, Z. Yu, Y. Ai, C. Li, Y. Kang, Z. Wang, Differential microfluidic sensor on printed circuit board for biological cells analysis, Electrophoresis. 36 (2015) 1854–1858.

50 C. Chen, J.H. Hahn, Dual-Channel Method for Interference-Free In-Channel Amperometric Detection in Microchip Capillary Electrophoresis, Anal. Chem. 79 (2007) 7182–7186.

51 J.H. Nieuwenhuis, F. Kohl, J. Bastemeijer, P.M. Sarro, M.J. Vellekoop, Integrated Coulter counter based on 2-dimensional liquid aperture control, Sens. Actuators, B. 102 （2004） 44–50.

52 R. Scott, P. Sethu, C.K. Harnett, Three-dimensional hydrodynamic focusing in a microfluidic Coulter counter, Rev. Sci. Instrum. 79, 046104 (2008).

53 Y.N. Xia, G.M. Whitesides, Soft lithography, Annu. Rev. Mater. Sci. 28 (1998) 153–184.

54 E. Weatherall, G.R. Willmott, Conductive and Biphasic Pulses in Tunable Resistive Pulse Sensing, J. Phys. Chem. B. 119 (2015) 5328–5335.

55 J. Menestrina, C. Yang, M. Schiel, Charged Particles Modulate Local Ionic Concentrations and Cause Formation of Positive Peaks in Resistive-Pulse-Based Detection, J. Phys. Chem. C. 118 (2014) 2391–2398.

56 G. Stober, L.J. Steinbock, U.F. Keyser, Modeling of colloidal transport in capillaries, J. Appl. Phys. 105, 084702 (2009).

57 L.J. Steinbock, G. Stober, U.F. Keyser, Sensing DNA-coatings of microparticles using

micropipettes, Biosens. Bioelectron. 24 (2009) 2423–2427.

58 E.C. Gregg, K.D. Steidley, Electrical Counting and Sizing of Mammalian Cells in Suspension, Biophys. J. 5 (1965) 393–405.

Table 1 Parameters used for simulation

Parameters	Values	Units
P	18.3	MΩ·cm
L_m	5.0	mm
L_d	5.0	mm
L_s	10.0	μm
D_m	19.1	μm
D_d	19.1	μm
D_s	6.7	μm

Table 2 Measured signals under different electric fields

Electric field (V/cm)	Average magnitude(V)	Standard deviation
6.7	0.0558	0.007967
13.4	0.1104	0.009342
18.9	0.1240	0.008756
25.2	0.1474	0.018787
32.4	0.1503	0.016131

Table 3 Measured signals by different particles

Particle diameter(μm)	Average magnitude (V)	Standard deviation
1	0.0216	0.003831
2	0.0282	0.007680
3	0.0768	0.009121
4	0.1432	0.012608
5	0.3080	0.051323
7	0.9261	0.301071

Figure Legends

Figure 1 The experimental system (a) and the configuration of the microfluidic chip (b).

Figure 2 The corresponding electric circuit model of the novel microfluidic RPS sensor without a particle (a) and with a particle at the entrance of the sensing gate (b).

Figure 3 Dependence of the output signal on (a) the relative resistance of the voltage input channels *a* (*b*=120,*c*=60,d=0.5), (b) the relative resistance of the detection channel, *b* (*a*=20,*c*=120,d=0.5) , (c) the relative resistance of the electric resistor, *c* (*a*=20,*b*=60,d=0.5) and (d) the relative resistance caused by the passing particle, d (a=20,b=120,c=60)

Figure 4 Typical trajectories of 5 μm around the sensing gate (a); Typical signals produced by particles passing by a sensing gate of 5×10×10 μm (width × length × height) (R_r=101KΩ), (b) 5μm particles, (c) 7μm particles. (The dashed line is the threshold to identify the particles) (E=20V/cm)

Figure 5 Typical signals by 1 μm particles passing by a sensing gate of 5×10×10 μm (width × length × height) (R_r=101KΩ) (a); the enlarged $1^{\#}$ signal (b); the enlarged $2^{\#}$ signal (c); the enlarged $3^{\#}$ signal (d). (The dashed line is the threshold to identify the particles) (E=20V/cm)

Figure 6 Signal magnitude distributions of 3 μm and 5 μm polystyrene particles

Figure 7 Typical detected signals for the a particle solution with 3 μm and 5 μm polystyrene particles with a sensing gate of 5×10×10 μm (width×length×height). (E=20V/cm)

Figure 8 Signal distribution of the mixed polystyrene particles sample

Figure 9 Typical signals created by 5 μm particles passing by a sensing gate of 5×10×10 μm (width × length × height) (R_r=101KΩ) when applying a voltage of 25.5V from Main channel 1(a); from both Main channel 1 and Main channel 2(b); from Main channel 1, 2 and 3 (c).

Figure 10 Dependence of the output signal on the electric field by a sensing gate of 5×10×21 μm (width × length × height) (R_r=101KΩ)

Figure 11 Dependence of the output signal on the particle size by a sensing gate of 5×10×10 μm (width × length × height) (R_r=101KΩ, E=20V/cm).

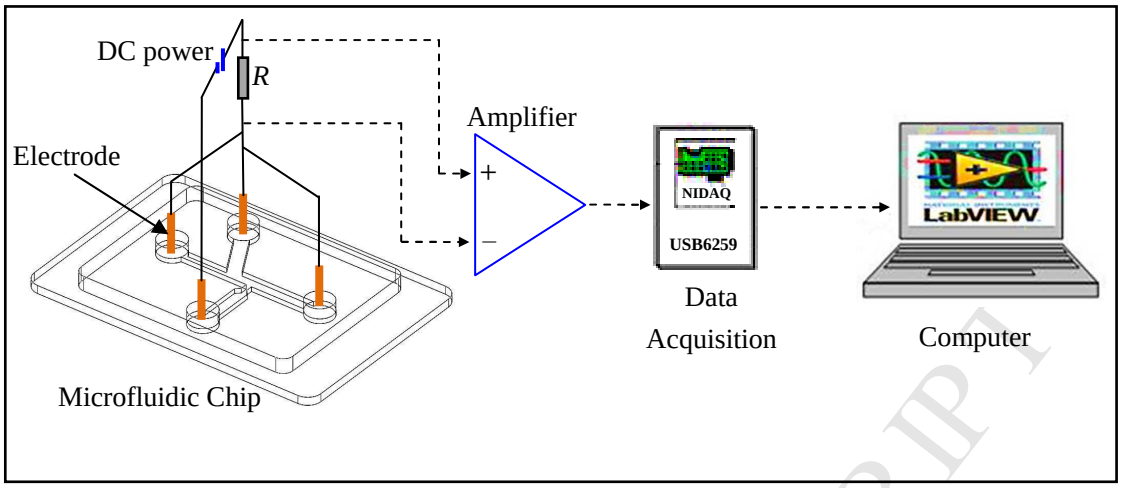
DC power
R
Electrode
Amplifier
+
–
NIDAQ
USB6259
Data
Acquisition
LabVIEW
Computer
Microfluidic Chip

(a)

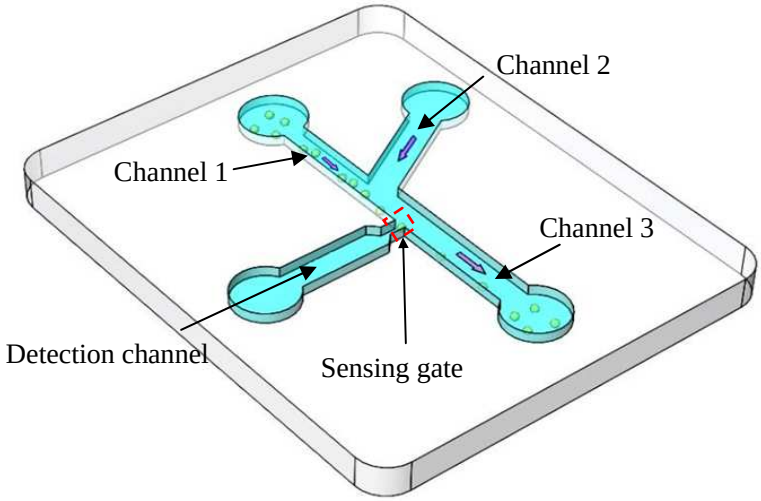
Channel 2
Channel 1
Channel 3
Detection channel
Sensing gate

(b)

Figure 1

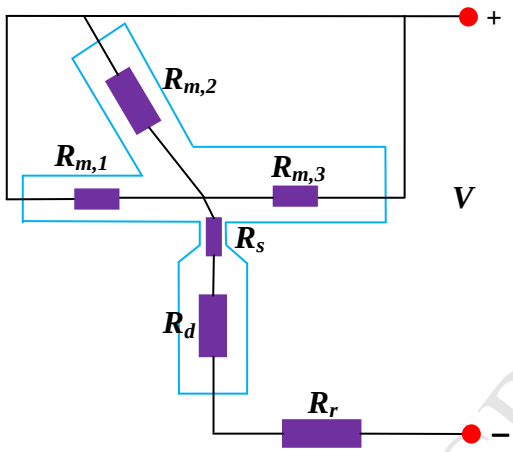

(a)

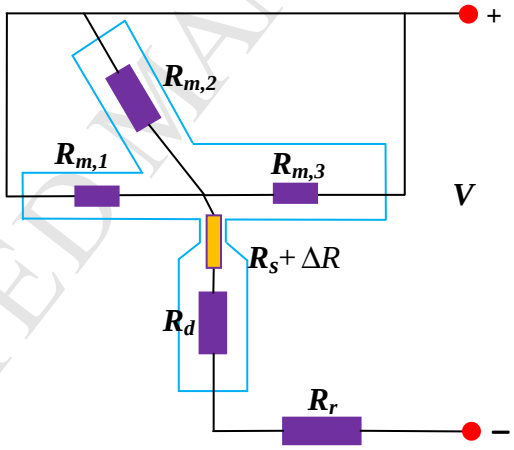

(b)

Figure 2

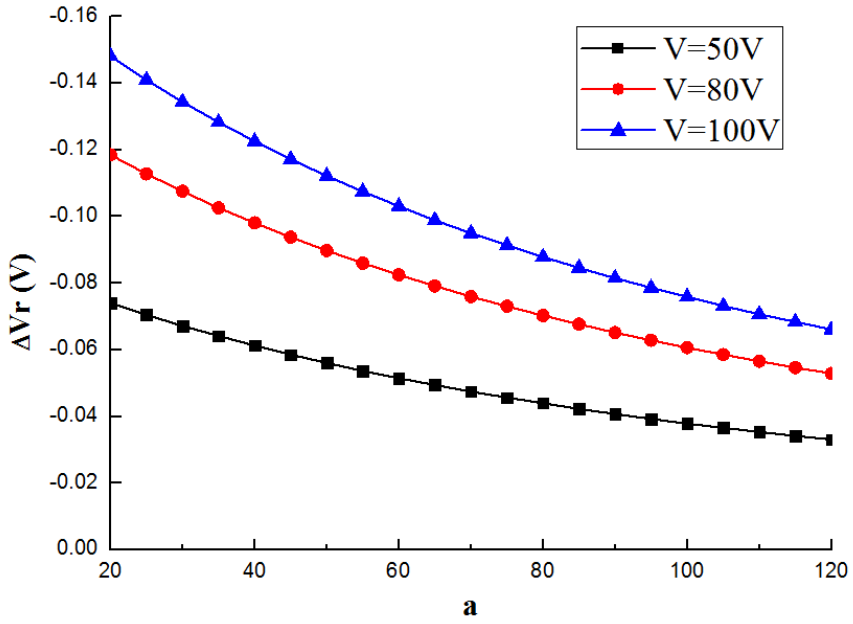
V=50V
V=80V
V=100V
ΔVr (V)
-0.16
-0.14
-0.12
-0.10
-0.08
-0.06
-0.04
-0.02
0.00
20
40
60
80
100
120
a

(a)

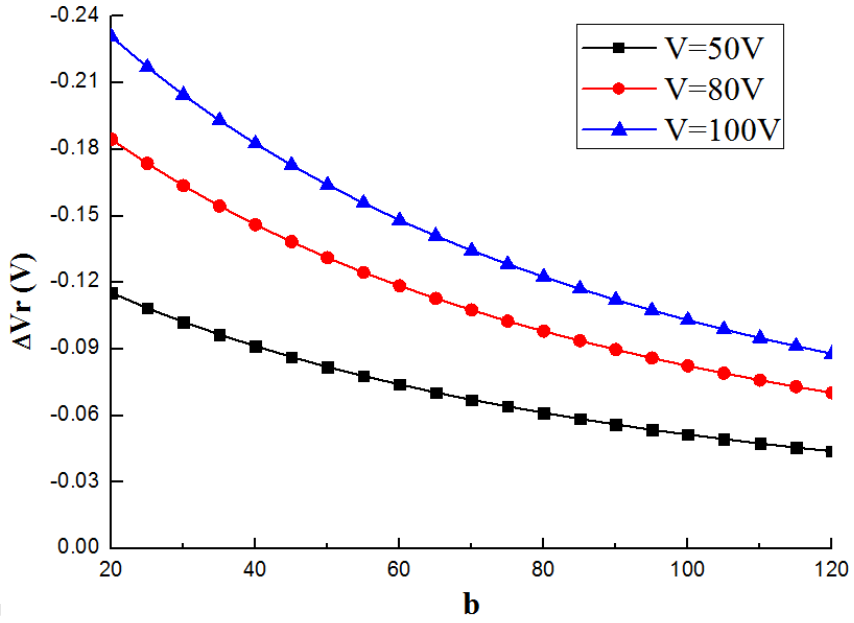
V=50V
V=80V
V=100V
ΔVr (V)
-0.24
-0.21
-0.18
-0.15
-0.12
-0.09
-0.06
-0.03
0.00
20
40
60
80
100
120
b

(b)

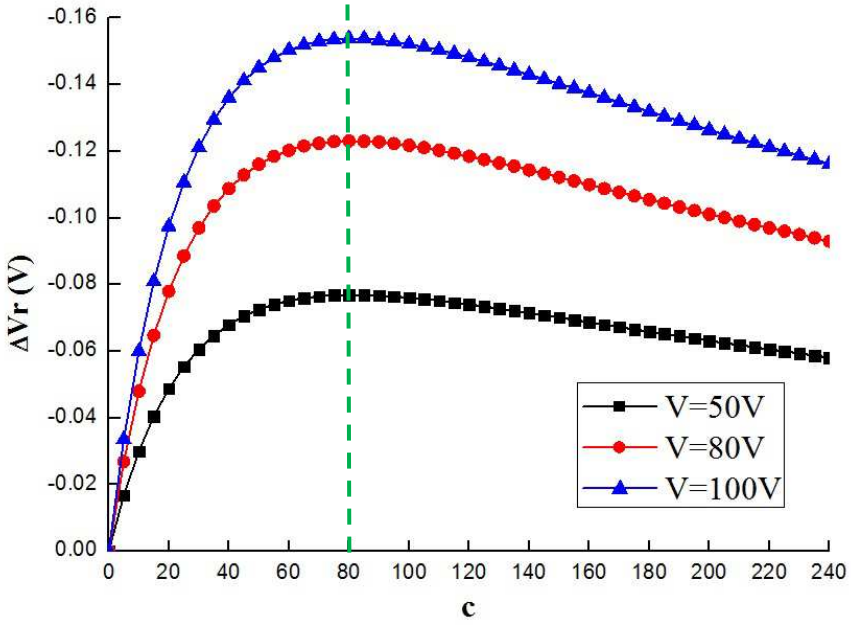
-0.16
-0.14
-0.12
-0.10
-0.08
-0.06
-0.04
-0.02
0.00
ΔVr (V)
0
20
40
60
80
100
120
140
160
180
200
220
240
c
V=50V
V=80V
V=100V

(c)

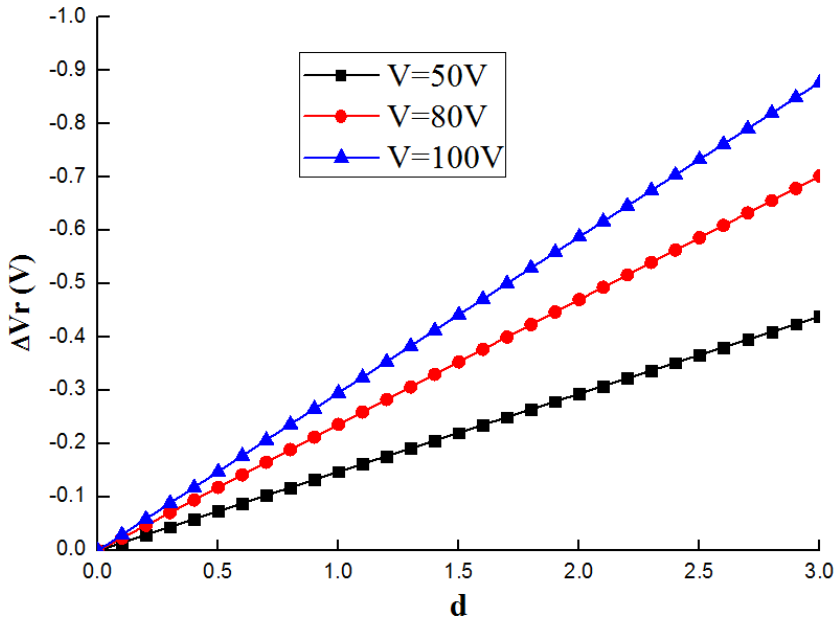
-1.0
-0.9
-0.8
-0.7
-0.6
-0.5
-0.4
-0.3
-0.2
-0.1
0.0
ΔVr (V)
0.0
0.5
1.0
1.5
2.0
2.5
3.0
d
V=50V
V=80V
V=100V

(d)

Figure 3

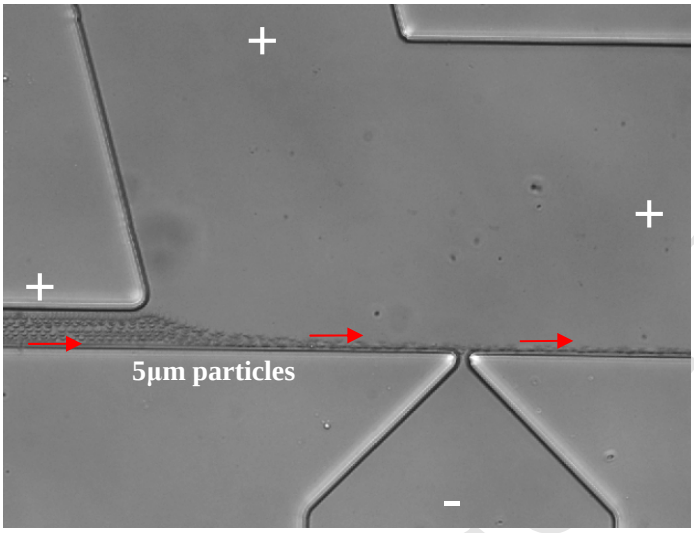

(a)

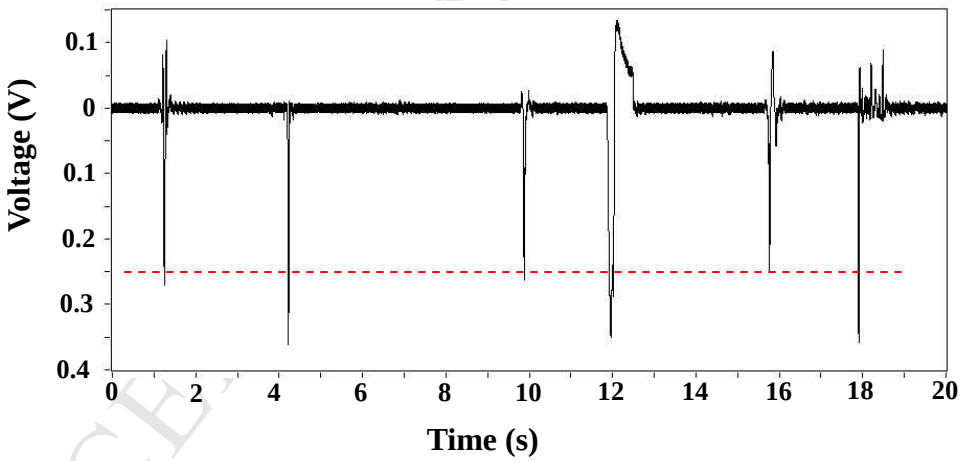

(b)

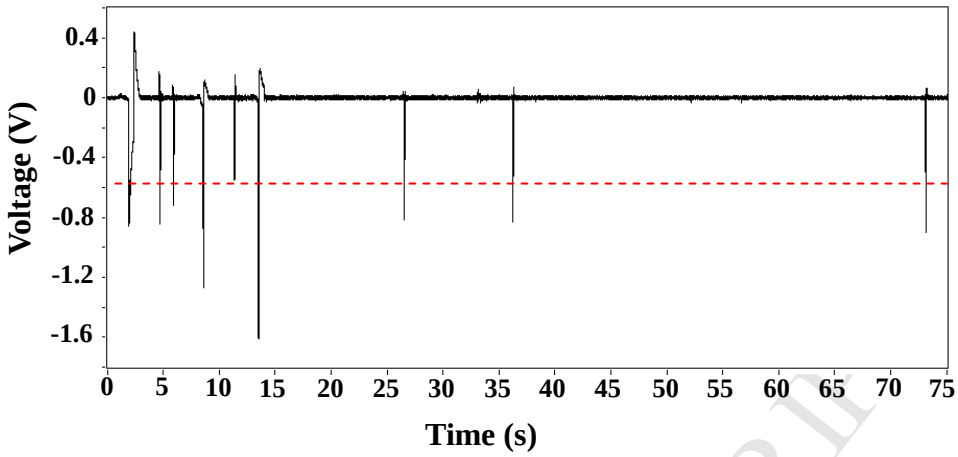

(c)

Figure 4

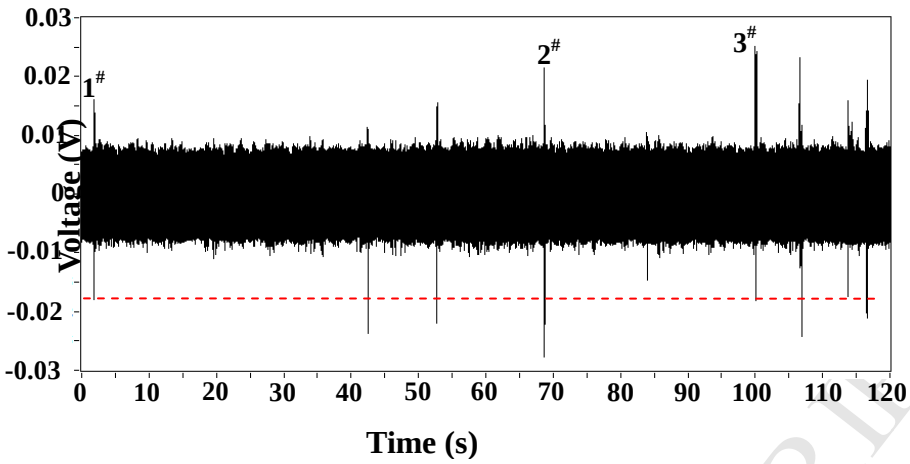

(a)

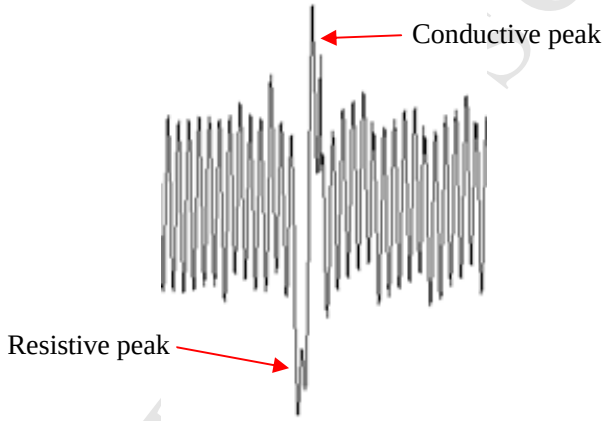

(b)

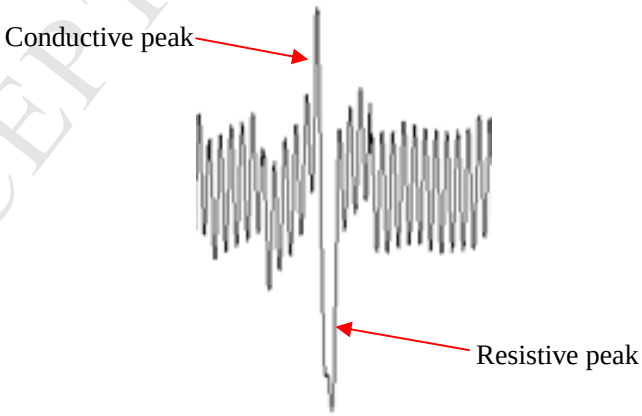

(c)

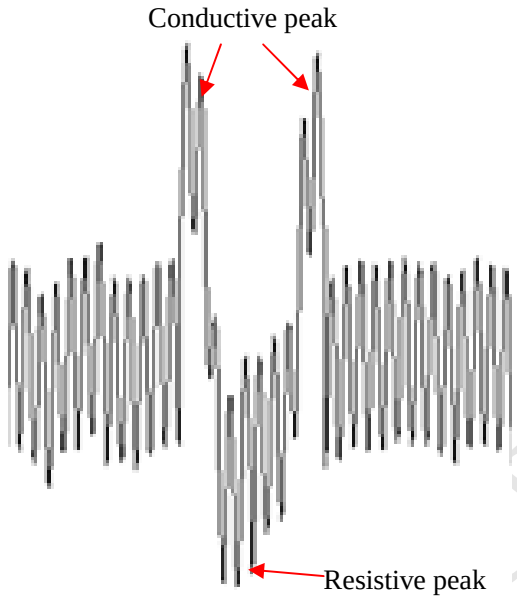

(d)

Figure 5

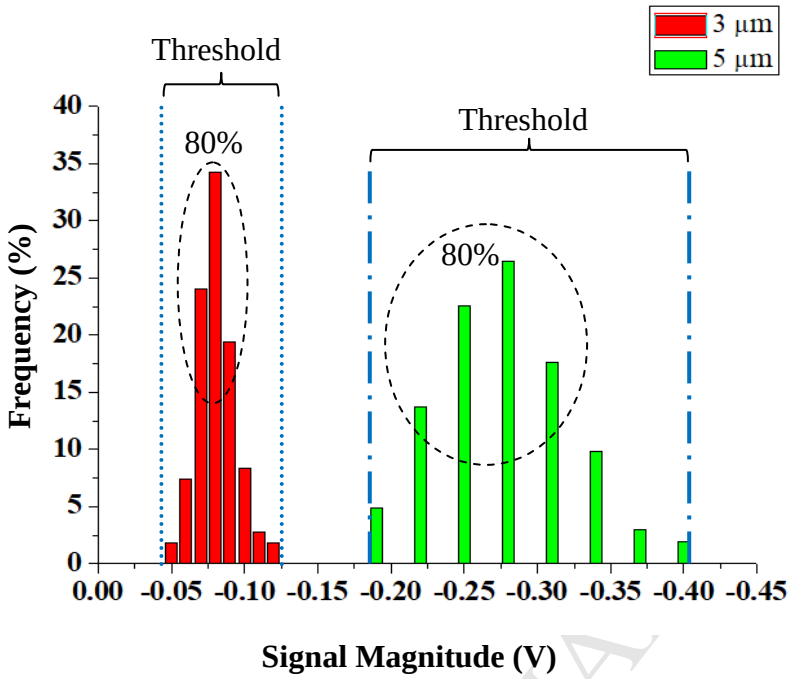

Figure 6

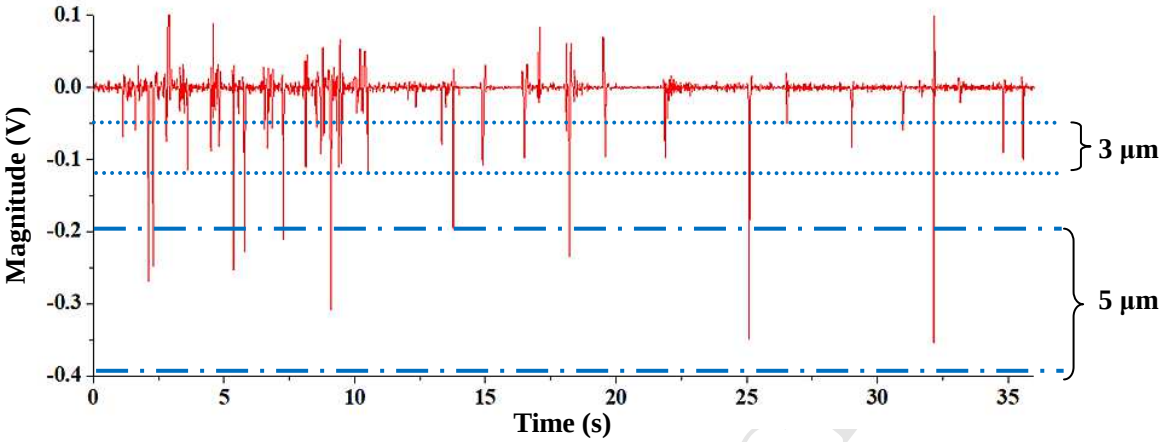

Figure 7

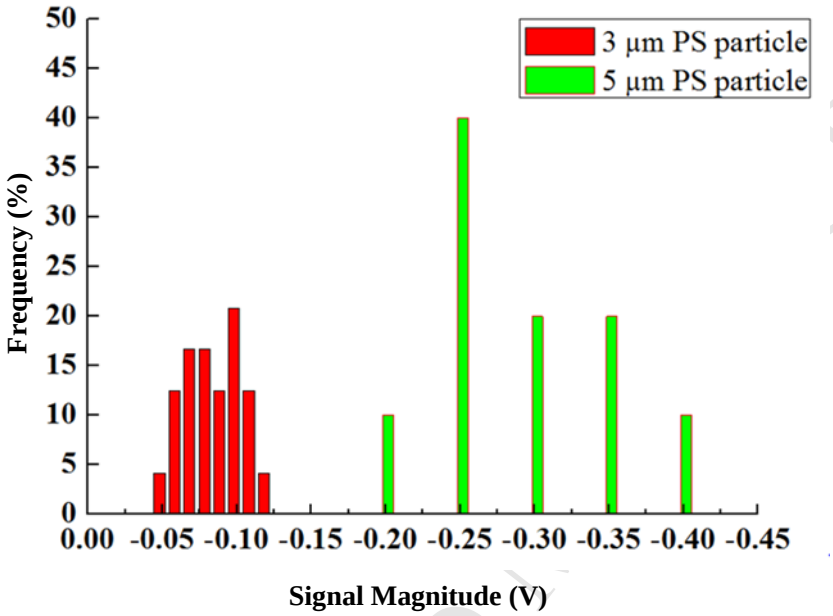

Figure 8

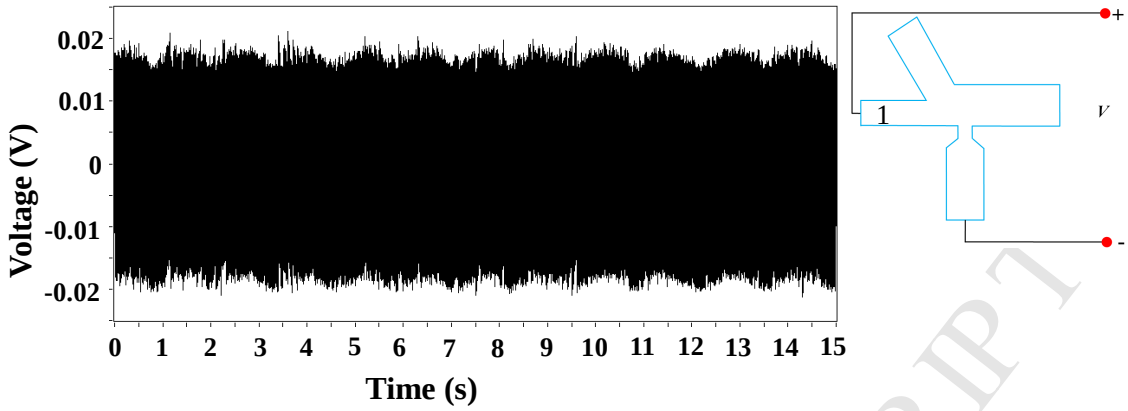
Voltage (V)
0.02
0.01
0
-0.01
-0.02
0 1 2 3 4 5 6 7 8 9 10 11 12 13 14 15
Time (s)
1
V
+
-

(a)

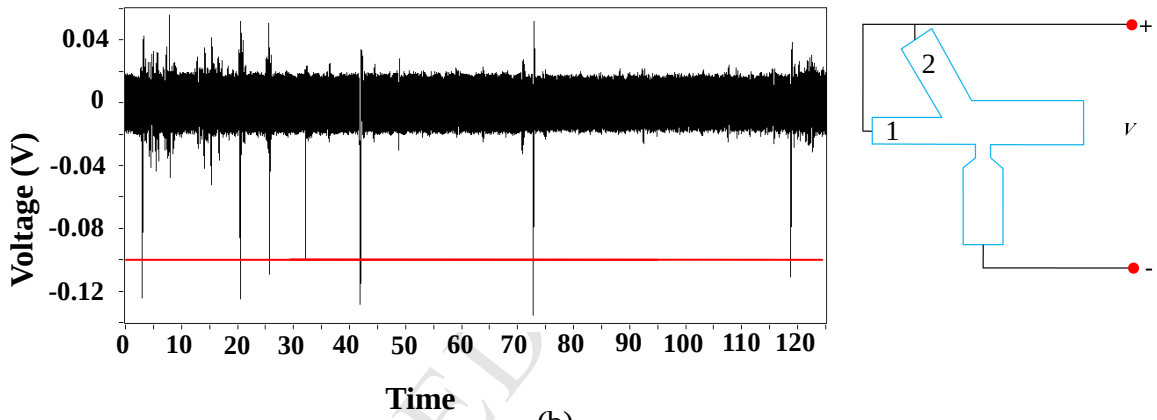
Voltage (V)
0.04
0
-0.04
-0.08
-0.12
0 10 20 30 40 50 60 70 80 90 100 110 120
Time
2
1
V
+
-

(b)

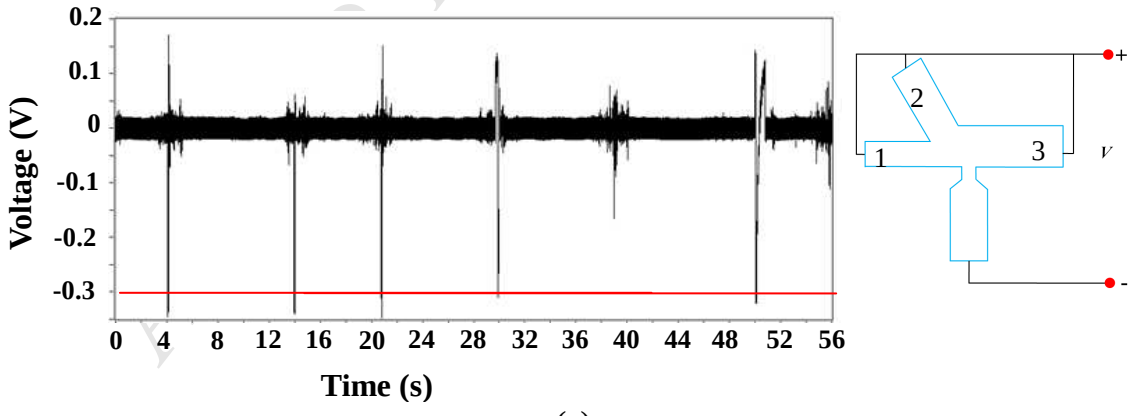
Voltage (V)
0.2
0.1
0
-0.1
-0.2
-0.3
0 4 8 12 16 20 24 28 32 36 40 44 48 52 56
Time (s)
2
1
3
V
+
-

(c)

Figure 9

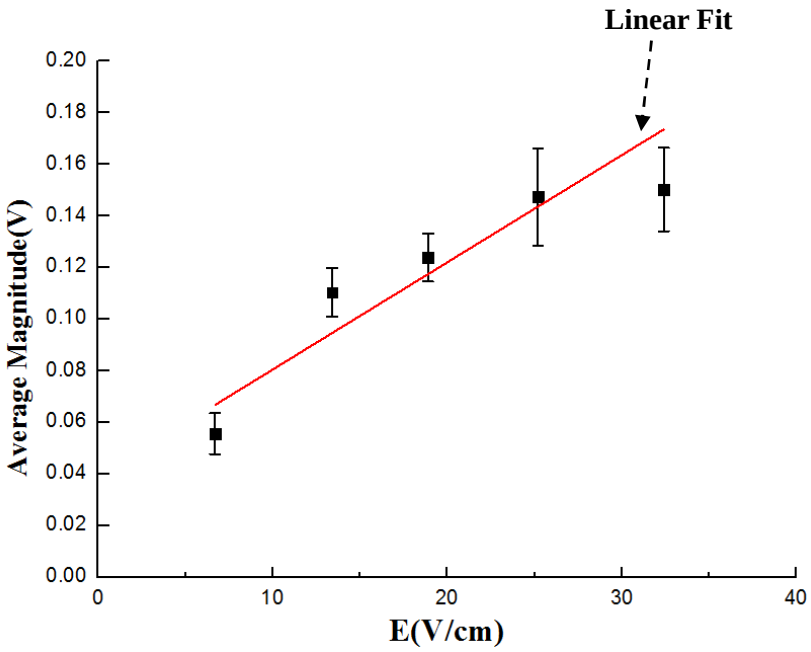

Figure 10

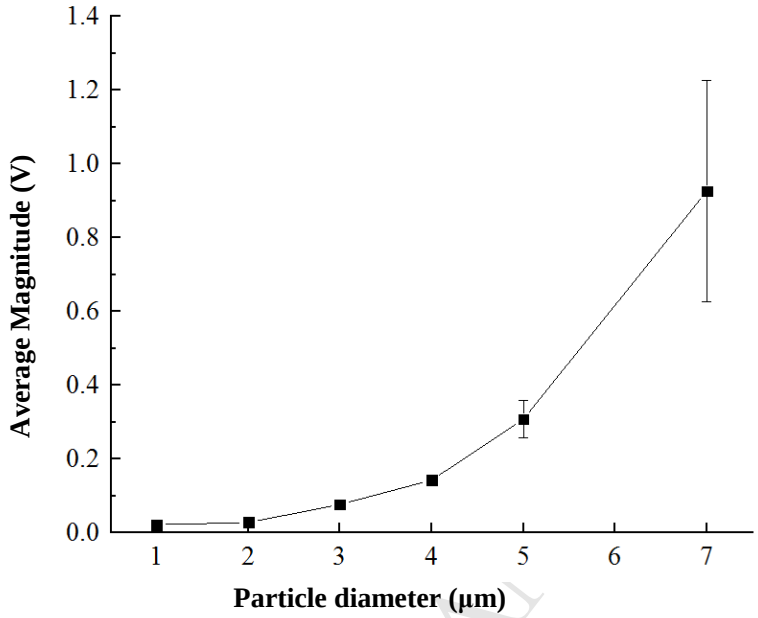

Figure 11

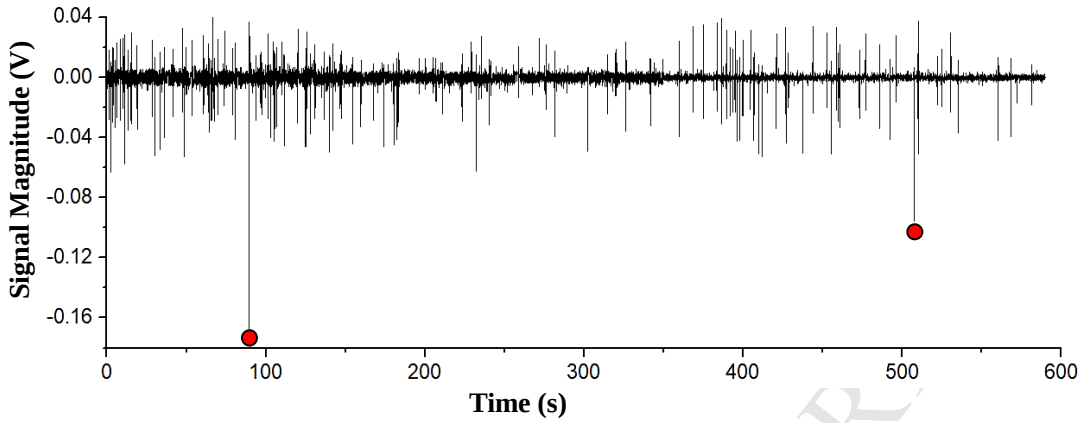
Signal Magnitude (V)
0.04
0.00
-0.04
-0.08
-0.12
-0.16
0
100
200
300
400
500
600
Time (s)

(a)

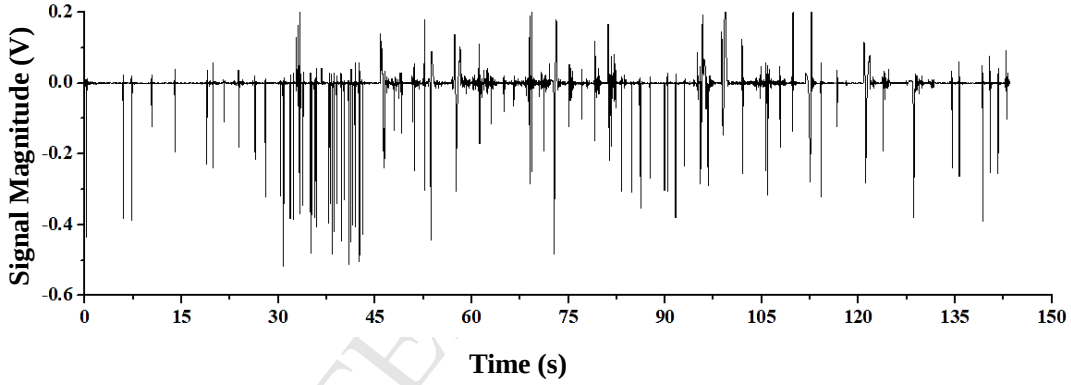
Signal Magnitude (V)
0.2
0.0
-0.2
-0.4
-0.6
0
15
30
45
60
75
90
105
120
135
150
Time (s)

(b)

Figure 12

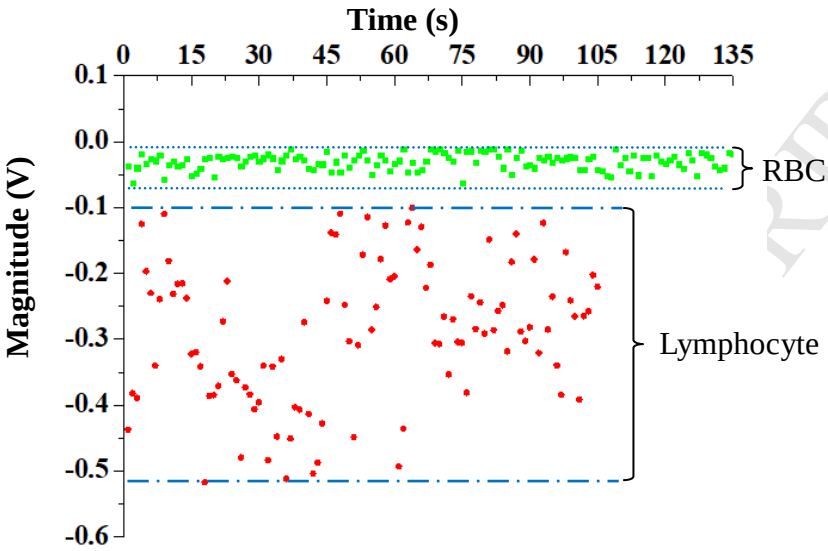

Figure 13

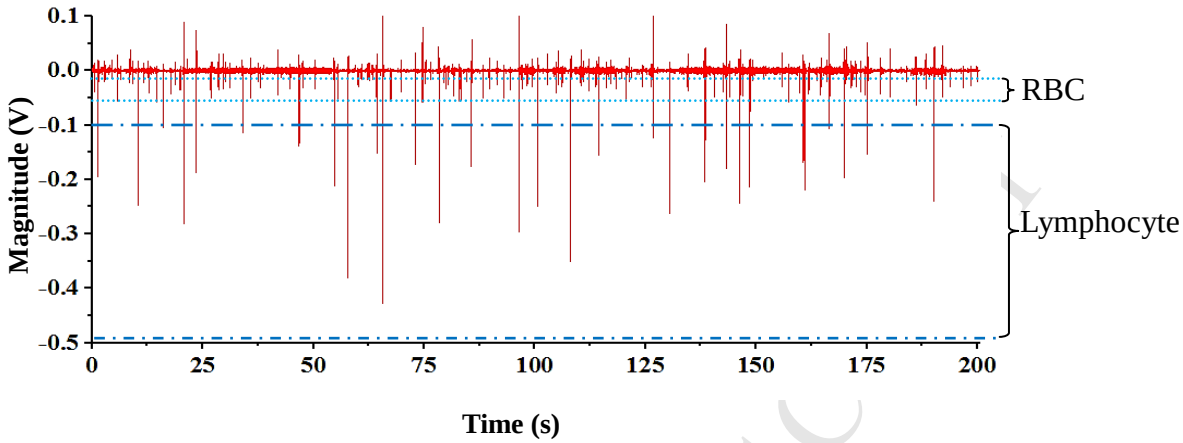

Figure 14

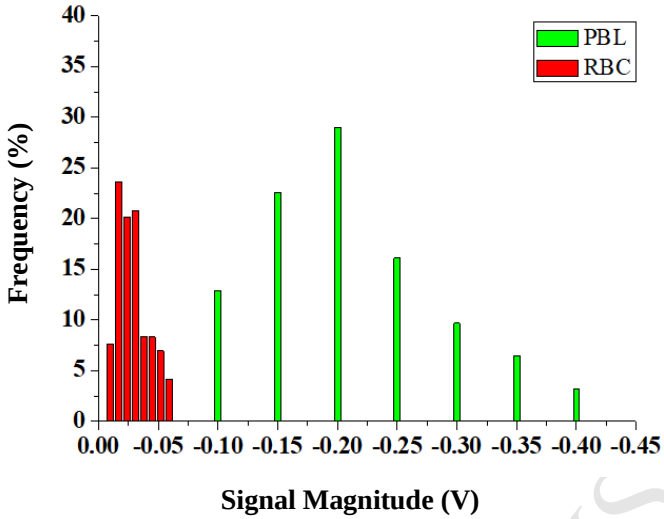

Figure 15

Highlights

- Particle and cell can be detected without passing through the sensing gate.
- Detection sensitivity can be tuned by changing the number of voltage input channels.
- Detection sensitivity can be tuned by changing the channel resistances.